Article

pubs.acs.org/Biomac

Size-Limited Penetration of Nanoparticles into Porcine Respiratory Mucus after Aerosol Deposition

Xabier Murgia,[†,‡] Paul Pawelzyk,[†,§] Ulrich F. Schaefer,[∥] Christian Wagner,[⊥] Norbert Willenbacher,[§] and Claus-Michael Lehr*[,‡,∥]

[‡]Helmholtz Institute for Pharmaceutical Research Saarland (HIPS), Helmholtz Centre for Infection Research (HZI), [∥]Biopharmaceutics and Pharmaceutical Technology, Department of Pharmacy, and [⊥]Experimental Physics, Saarland University, 66123 Saarbruecken, Germany

[§]Institute for Mechanical Process Engineering and Mechanics, Karlsruhe Institute of Technology (KIT), 76131 Karlsruhe, Germany

Supporting Information

ABSTRACT: We investigated the rheological properties and the penetration of differently sized carboxylated nanoparticles in pig pulmonary mucus, on different distance and time scales. Nanoparticles were either mechanically mixed into the mucus samples or deposited as an aerosol, the latter resembling a more physiologically relevant delivery scenario. After mechanical dispersion, 500 nm particles were locally trapped; a fraction of carboxylated tracer particles of 100 or 200 nm in diameter could however freely diffuse in these networks over distances of approximately 20 μm. In contrast, after aerosol deposition on top of the mucus layer only particles with a size of 100 nm were able to penetrate into mucus, suggesting the presence of smaller pores at the air-mucus interface compared to within mucus. These findings are relevant to an understanding of the fate of potentially harmful aerosol particles, such as pathogens, pollutants, and other nanomaterials after incidental inhalation, as well as for the design of pulmonary drug delivery systems.

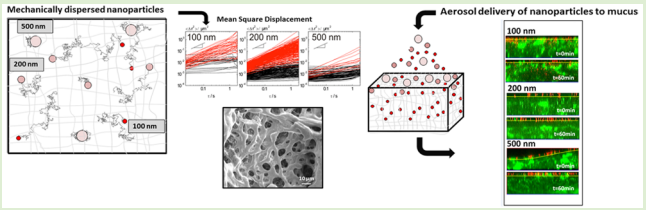

INTRODUCTION

Mucus is a complex hydrogel that provides tissue lubrication, first-line defense, and residual material clearance in the mucosal tissues of the human body, including the pulmonary airways, the gastrointestinal tract, the genitourinary tract, and the ocular surface.[1−3] In the lungs a mucus layer coats the conducting airways. Gel-forming mucins are continuously secreted into the airway lumen and incorporated into a high-viscosity, gel-like mucus layer,[4,5] which is continuously propelled toward the trachea and finally cleared from the lungs.[5] The highly dynamic nature of the mucociliary machinery therefore confers the ability to entrap and eliminate inhaled particles in a short time window ranging from minutes to a few hours, with clearance rates in the order of 100 μm/sec.[6] In the context of aerosol medicine and pulmonary drug delivery, the protective barrier properties of mucus against inhaled pathogens and pollutants may therefore impose a significant challenge, in particular, for nanoparticles intended for use as therapeutic drug carriers.[7]

Bulk rheological studies conducted within the linear viscoelastic region, where the structural properties of mucus are unaffected by the macroscopic shear deformation, show that pulmonary mucus behaves as an elastic solid on the macroscopic level.[3,8,9] Direct information on nanoparticle-mucus interactions can be obtained by tracking the Brownian motion of tracer particles, that is, using microrheological methods.[10−12] Mucus can adsorb particles due to electrostatic and hydrophobic attractive forces (interaction filtering).[13,14] Noninteracting nanoparticles with a smaller size than the pore size of the mucus can diffuse freely through the pores, in contrast to particles of bigger size that are confined by the surrounding mucin fibers (steric filtering).[12] Particle tracking investigations have revealed that the microscopic structure of mucus is highly heterogeneous, showing that within the same submicron particle size range freely diffusing particles coexist with particles which are immobilized by the mucus gel. These studies highlight that the overall particle mobility depends on mucus composition,[8,15] as well as particle diameter[3,16] and surface functionality.[3,10,17] In the case of human pulmonary mucus, most particles with a size of 500 nm are immobilized,[3,16] whereas, for smaller particles in the size range of 100−200 nm, the fraction of diffusing particles can be significantly increased if the surface of the particles is densely coated with polyethylene glycol (PEGylation).[3] The same studies however demonstrated that a fraction of carboxylated 100 and 200 nm particles still diffused within pulmonary mucus, indicating that interaction filtering is not the only mechanism.[3,16]

The starting point for the present study was the intriguing observation that magnetic nanoparticles did not penetrate a capillary filled with pulmonary mucus under application of a magnetic field, while the same particles penetrated a hydroxyl-ethyl-cellulose (HEC) hydrogel with apparently similar

Received: February 3, 2016
Revised: March 4, 2016
Published: March 9, 2016

DOI: 10.1021/acs.biomac.6b00164
Biomacromolecules 2016, 17, 1536−1542

viscoelastic properties under the same conditions rather easily.[18] Subsequent cryogenic-scanning electron microscope studies revealed a cage-like structure of the native mucus hydrogel, with both micron- as well as submicron-sized pores. This observation brought us to a new hypothesis: While the partly contradictive reported results regarding particle mobility and transport within and through mucus are clearly a reflection of particle size and surface properties,[3,19,20] differences in the time and distance scales employed within the conducted experiments may also play a role. The transport over longer distances, but at the same time rather free, Brownian-like mobility of some nanoparticles over shorter distances, can probably be best explained by the peculiar structure of the mucus gel network, which is also reflected in the different macro and microrheological properties of native mucus.[18]

In this study, we therefore investigated the linear viscoelastic properties of mucus and the mobility of particles over different distance and time scales, using carboxylated polystyrene particles of different sizes (100, 200, and 500 nm) as model systems. Multiple particle tracking (MPT), in which particle displacement is followed over short time-scales (usually up to 10 s), was used to study the diffusion on the microscale (0.1−1 μm). Fluorescence recovery after photobleaching (FRAP) experiments were used to elucidate particle mobility through mucus on time (760 s) and distance (bleached area of 35 μm) scales closer to therapeutic scenarios.[2,21] After deposition in the airways, for example, when inhaled as aerosols within droplets or carrier particles, with an adequate aerodynamic particle size in the micron range (a typical scenario in pulmonary drug delivery), administered nanoparticles have to travel 3−50 μm to traverse the mucus layer before reaching the epithelial cell surface.[6,22] The time scale for penetration is determined by the highly dynamic mucociliary machinery, that is, several minutes up to a few hours.[6] We therefore tried to correlate the corresponding diffusion data for differently sized particles with the penetration of nanoparticles within mucus or across the air-mucus interface, in an attempt to model a more realistic scenario for nanoparticle-based drug delivery to the airways. Most importantly, we found a striking difference between the mobility of particles within mucus after mechanical dispersion and the penetration of the same particles into mucus after deposition as an aerosol.

MATERIALS AND METHODS

Mucus Sample Collection. Native porcine pulmonary mucus was obtained from the tracheas of slaughtered pigs, sourced from a local slaughterhouse. Approximately 10 cm of windpipe was isolated in each case by cutting the trachea below the larynx and before the carina. Tracheas were stored on ice for further transport and mucus extraction. Prior to extraction procedures tracheas were cut in half longitudinally. The mucus was gently scratched from the luminal surface with a spatula (approximately 100−300 μL of mucus per sample). For MPT and shear rheology experiments, mucus samples were stored at 4 °C, and experiments were conducted within 12−36 h of mucus collection. Remaining mucus samples were stored at −20 °C until further analysis.

Shear Rheology. Experiments were conducted on a Thermo MARS II rheometer equipped with cone−plate geometry (diameter, 35 mm; cone angle, 1°) at room temperature. The edges of mucus samples were coated with a low viscosity paraffin oil to prevent sample evaporation. Strain amplitude sweeps were performed at a frequency of 1 Hz. Frequency dependency of the storage modulus G' and the loss modulus G'' was measured in the range between 0.01 and 10 Hz at strain amplitudes of $\gamma \leq 0.1$. The characterization of the bulk rheological properties of mucus was based on independent measurements of four different samples.

Multiple Particle Tracking (MPT). Carboxylated, green-fluorescent polystyrene microspheres with diameters of 100, 200, and 500 nm (Bangs Laboratories, U.S.A.) were used in MPT experiments. Particle diameters, polydispersity indices (PdI) and zeta potential (ζ) were measured prior to MPT studies, using a Malvern Zetasizer Nano ZSP or a Zetasizer Nano ZS (Malvern, U.K.; Table 1).

Table 1. Particle Characterization

nominal particle size	diameter[a] (d) nm	polydispersity index[b] (PdI)	surface charge density[c] charges/nm^2	ζ-potential[d] mV
100 nm	112 ± 1	0.02 ± 0.01	3.0	−49 ± 4
200 nm	221 ± 2	0.01 ± 0.01	1.9	−57 ± 4
500 nm	524 ± 10	0.07 ± 0.05	14.6	−34 ± 2

[a]Z-average diameter measured by dynamic light scattering. Standard deviation is based on six independent measurements. [b]PdI = $(\sigma/d)^2$ calculated from the Z-average diameter (d) and the standard deviation of the particle size distribution. [c]Provided by the manufacturer. [d]Measured in 10 mM NaCl at pH 7.4.

Approximately 20 μL of fresh mucus sample was then mixed with 0.5 μL of the particle dispersions. The 500 nm particles were used at the original particle concentration of 1% w/v. Dispersions of the smaller particles were diluted with PBS buffer to obtain particle concentrations of 0.05% w/v for 100 nm and 0.25% w/v for the 200 nm particles, thus keeping the number concentration of particles below $2-10^{10}$ particles/ml in all cases. The whole sample was then transferred to a custom-made chamber, sealed, and placed in the microscope.[23] Measurements were performed using an inverted fluorescence microscope (AxioObserver D, Zeiss, Germany) with a Fluar 100× objective and an oil-immersion lens with a numerical aperture of 1.3. The temperature was maintained at 37 °C using a temperature controlled chamber. Tracking videos of random fields of each mucus sample were recorded by an sCMOS camera Zyla X (Andor Technology), at a resolution of 0.062 μm per pixel and a frame rate of 50 frames per second. The field of view of the camera represents an area of 127 × 127 μm. Image analysis was conducted using Image Processing System software (Visiometrics iPS). The data were evaluated as described by Kowalczyk et al.[23]

Fluorescence Recovery after Photobleaching (FRAP). Previously frozen native pulmonary mucus samples were thawed at 4 °C the day prior to FRAP experiments. The following day, samples were allowed to reach room temperature and thereafter 60 μL of mucus was mixed with 1.5 μL of the particle dispersions. Mixtures of mucus and tracer particles were prepared as mentioned above for the MPT experiments, using the same carboxylated green-fluorescent polystyrene microspheres at the previously stated concentrations. These nanoparticle concentrations were all within the range where a linear relationship exists between concentration and fluorescence (Supporting Information, 1). The samples were then transferred into previously mounted adhesive gastight sealing chambers (Gene Frame, Thermo Scientific), and sealed with cover slides. The experiments were conducted using a LSM 710 Axio Observer confocal laser scanning microscope (Zeiss, Germany) with an Apochromat 40×/1.1 objective equipped with a 488 nm laser (LASOS RMC 7812 Z2). The temperature of samples was maintained at 37 °C using a temperature controlled chamber. Four circular regions of interest (radius = 17.5 μm in all cases) were selected within the analyzed field, of which three were used for bleaching experiments and one was retained as a control for photofading. A time-series analysis was programmed with the following settings: Prebleaching images were recorded at 2% laser transmission, immediately followed by bleaching with the laser transmission set at 100%. A postbleaching recovery step followed, for a duration of 760 s at a frame rate of 30 frames per minute with the laser transmission again set at 2%. The fluorescence intensity after bleaching was defined as zero, and the intensity at $t = 0$ was subtracted

DOI: 10.1021/acs.biomac.6b00164
Biomacromolecules 2016, 17, 1536−1542

from all values. Arbitrary values of intensity were then calculated, dividing each obtained value by the difference between the intensities prior to and directly after bleaching. The results were further corrected for the intensity of the control area. The presented data were extracted from four independent bleaching experiments per particle size.

Aerosol Delivery of Nanoparticles and Confocal Microscopy. Carboxylated red-fluorescent polystyrene nanoparticles of 100, 200, and 500 nm diameter (Invitrogen, stock 2%) were dispersed in PBS at 0.1%, 0.025% and 0.005% w/v, respectively. Frozen native pulmonary mucus samples were thawed at 4 °C the day prior to experiments. A 40 μL volume of mucus was then stained by gentle mixing with 1 μL of Alexa488 Wheat Germ Agglutinin (Vector Laboratories, CA, U.S.A.), and transferred to an imaging chamber to create a confluent mucus layer.

Nanoparticle suspensions were aerosolized using a micropump nebulizer (AerogenLab, Aerogen Ltd., Ireland, droplet size range 2.5−4 μm). The nebulizer was aligned 6 cm above the mucus-containing imaging chamber and 20 μL of nanoparticle suspension was aerosolized over the sample, allowing 2 min for particle deposition. The sample was then transferred to the confocal laser scanning microscope (LSM 710 Axio Observer Zeiss, Germany) with an Apochromat 40×/1.1 objective to study the time-dependent vertical penetration of the particles through mucus. The temperature was maintained at 37 °C using a humidified and temperature controlled chamber. The stained mucus was detected in the green channel (excitation 488 nm, detection 467−554 nm) and the fluorescent nanoparticles in the red channel (excitation 561 nm, detection 624−707 nm). Once the surface of the mucus sample was located, *Z*-stacks encompassing 30−50 μm of the mucus layer were imaged (t = 0 min). The procedure was repeated after 1 h (t = 60 min).

RESULTS AND DISCUSSION

2.1. Bulk Rheology. The frequency dependence of the viscoelastic properties of bulk mucus samples in the linear viscoelastic region is shown in Figure 1. The error of these

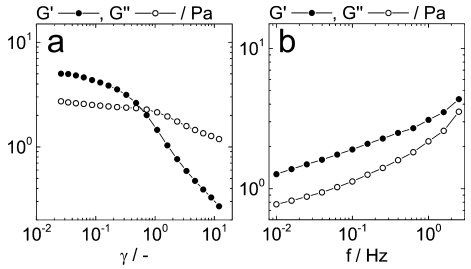

Figure 1. Representative amplitude sweep experiment at a frequency f = 1 Hz (a), and frequency sweep experiment at a strain γ = 0.1 (b).

measurements, calculated from four independent experiments, is below 10%. As expected, the storage modulus G' was found to be larger than the loss modulus G'' in the frequency range between 0.01 and 3 Hz, while the ratio of the loss modulus and the storage modulus ($\tan(\delta) = G''/G' \approx 0.6$ at a frequency of 0.159 Hz. Both moduli are only weakly frequency dependent in the investigated frequency range. These characteristics are typical of cross-linked gels or sample-spanning particle networks.[23] Tracheal mucus obtained from humans or other animal models exhibits similar bulk rheological properties.[3,9,24] The amplitude sweep performed at a frequency of 1 Hz shows that the mucus layer is a weak gel which starts to soften already at deformations around $\gamma \approx 0.05$. The sample yields at deformations of $\gamma = 0.6$, as indicated by the crossover of G' and G''.

2.2. Multiple Particle Tracking (MPT). Investigations into the pulmonary mucus pore size have shown significant variability in the pore dimensions of the mucin network, ranging from pores of a few nanometers to voids in the micrometer size range.[3,18,25] Pore size estimations, however, have often been derived from scanning electron microscopy, and might therefore be biased by the mandatory fixation and dehydration steps. MPT, on the other hand, provides information on the mucus architecture with minimal manipulation of the sample. The mean squared displacement (MSD) $\Delta r(\tau)^2$ in native pulmonary mucus for 100 nm, 200 and 500 nm carboxylated polystyrene particles shows a broad distribution irrespective of particle size, indicating that mucus samples are heterogeneous on this scale (Figure 2; Supporting Information, videos 1−3).

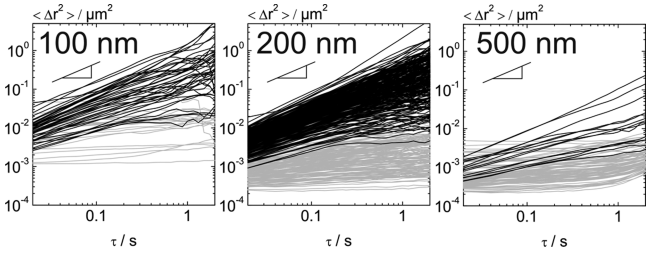

Figure 2. Mean squared displacement (MSD, $\langle \Delta r^2 \rangle$) of carboxylated nanoparticles in pulmonary pig mucus as a function of time τ. Black lines represent MSDs with a slope $\alpha > 0.5$, classified as diffusive, while gray lines denote MSDs with $\alpha < 0.5$, classified as immobile. The gradient triangle in each figure illustrates a slope of 1.

Therefore, instead of analyzing the average $\langle \Delta r(\tau)^2 \rangle$ for a collection of particles, we analyzed the slope $\alpha = d \log(\Delta r(\tau)^2)/d \log(\tau)$ of each individual MSD and classified each particle as either diffusive or immobile according to its α-value. This scaling exponent describes the diffusive properties of the particles; for Newtonian fluids $\alpha = 1$, while $\alpha = 0$ in purely elastic materials. We used a cutoff value of 0.5 to classify the particles as diffusive ($\alpha > 0.5$) or immobile ($\alpha < 0.5$). The classification as shown in Figure 2 is based on α-values obtained at $\tau = 0.1$ s. However, classification according to the $\alpha = 0.5$ criterion is essentially independent of τ. The slope of the MSDs of the diffusive (black lines) and the immobile particle fraction (gray lines) is either approximately zero or close to one, respectively.

MSDs increasing linearly with time (Figure 2, black lines) correspond to a constant diffusion coefficient as typical for Newtonian fluids. The corresponding particles move freely through the fluid within the pores of the mucin network, and their diffusion coefficient can be directly calculated according to

$$\Delta r^2(\tau) = 4D\tau \tag{1}$$

The viscosity of fluid surrounding these particles can be estimated from the diffusion coefficient D and the particle diameter d, using the Stokes−Einstein equation:

$$\eta = \frac{k_B T}{3d\pi D} \tag{2}$$

with k_B denoting the Boltzmann constant and T is the absolute temperature. This simple relationship is valid for particles diffusing in an infinitely viscous environment.

The broad variation of MSDs is an intrinsic characteristic of the heterogeneous mucus microstructure. Hence, rather than using the mean values of collective particles, we decided to focus on the 10th and 90th percentiles of the MSD fractions

DOI: 10.1021/acs.biomac.6b00164
Biomacromolecules 2016, 17, 1536−1542

classified by the slope criterion, as depicted in Figure 2, to proceed with calculation of the related physical parameters, namely, the diffusion coefficient D of the tracer particles, and the effective viscosity η in the viscous regions. These interpercentile ranges therefore represent the viscoelastic properties traced by 80% of the particles. Results based on these considerations and corresponding numerical values are summarized in Table 2.

Table 2. Range of Physical Properties in Relation to 100, 200, and 500 nm Particles within the Viscous Mucus Fractions

	viscous fraction	
particle size	diffusion coefficient D (10^{-13} m^2/s)	viscosity η (mPa s)
100 nm	0.46−22	2−90
200 nm	0.12−1.7	12−175
500 nm	[a]	
overall range	0.12−22	2−175

[a]Number of diffusive particles too small for a reasonable calculation of D or η. With n = 3 measurements, each performed on an independent mucus sample.

The distribution of the slopes of the individual particle MSDs at τ = 0.1 s, calculated from three independent samples, is shown in Figure 3. The 100 and 200 nm particles exhibit a

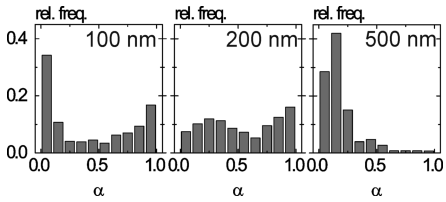

Figure 3. Histograms depict the slope $\alpha = d\log(\mathrm{MSD})/d\log(\tau)$ of the MSDs at a time scale τ = 0.1 s, averaged from the relative frequencies of three measurements, each performed on an independent mucus sample.

broad distribution, whereas mainly immobile particles with $\alpha <$ 0.5 were observed at a particle diameter of 500 nm. According to the selected classification criterion, 43, 51, and 6% of 100, 200, and 500 nm particles, respectively, were found to be diffusive, that is, moving in a viscous environment.

Our MPT data shows that mucus is an extremely heterogeneous, viscoelastic material consisting of viscous regions, termed pores, and highly elastic areas thought to consist of a dense polymeric network. The mesh size of this network seems to be smaller than 100 nm in some areas (since even 100 nm particles are trapped). On the other hand, essentially all 500 nm particles are found to be in an elastic environment, that is, they cannot enter the porous regions and as a result the pore size is estimated to be smaller than 500 nm. The limited diffusion of particles above this cutoff size within pulmonary mucus is directly linked to the pore size of the mucin network, and is independent from particle-mucin chemical interactions since even 500 nm particles coated with a dense layer of PEG, which significantly reduces the adsorption of biomolecules on particle surfaces, are immobilized within the mucin network.[3]

2.3. Fluorescence Recovery after Photobleaching (FRAP). In a subsequent step, FRAP experiments were performed to determine the transport of particle populations on longer time (720 s) and distance scales. We conducted these experiments with mucus stored at −20 °C after having found equivalent results in terms of mobility for 100 and 200 nm particles during pilot MPT experiments with fresh or slow-thawed porcine pulmonary mucus (Supporting Information, 4). FRAP experiments confirmed the low mobility of the 500 nm particles. The fluorescence recovery for 500 nm particles was very modest, barely reaching 10% recovery within the experimental time, indicating that these particles were mostly immobile (Figure 4).

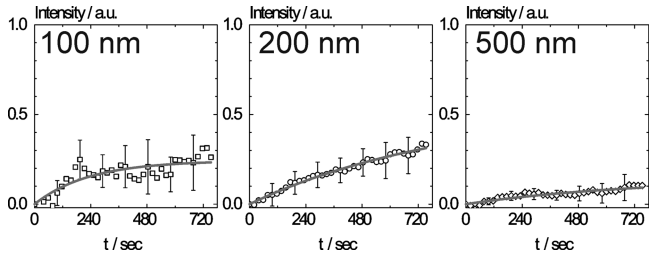

Figure 4. Fluorescence intensity recovery over time t determined from FRAP experiments using 100 (squares), 200 (circles), and 500 nm (diamonds) particles and the corresponding exponential fits (gray line). With n = 12, from four independent samples.

As expected, 100 and 200 nm particles showed a higher fluorescence recovery than 500 nm particles within the time frame of the experiment, which was approximately 760 s. Nevertheless, at this time the mobile particle fraction depicted by the mean fluorescence recovery was higher for the 200 nm (33%) than for the 100 nm (26%) particles.

In order to obtain further information regarding the diffusion of the nanoparticles in native pulmonary mucus, the following exponential function was fitted to the data of the arbitrary intensities I:

$$I(t) = A(1 - e^{-\tau t}) \quad (3)$$

The parameter A corresponds to the estimated fraction of mobile particles. The time constant τ is a characteristic of the intensity increase over time and can be used to calculate the halftime recovery $\tau_{1/2}$:

$$\tau_{1/2} = \ln(2)/\tau \quad (4)$$

The diffusion coefficient can then be obtained from the halftime recovery and the radius of the bleached area (w = 17.5 μm) following the approach of Axelrod et al.:[26]

$$D = 0.88w^2/4\tau_{1/2} \quad (5)$$

The diffusion coefficients for the differently sized particle samples yielded values in accordance with those obtained for the most diffusive particles during the MPT experiments (Table 3).

We observed a higher diffusion coefficient in pulmonary mucus for 100 nm particles in comparison to the larger ones, suggesting a critical mucus pore size between 100 and 200 nm. According to our data (Figure 4) and the applied model (Table 3), the mobile fraction of the 100 nm particles (24%) was also larger than that of the 500 nm particles (14%). Surprisingly, however, the model yielded a mobile fraction for the 200 nm particles (around 50%), which was even higher than for both the larger 500 nm and smaller 100 nm particles. By applying the model described by Axelrod et al. to the FRAP data, we were

DOI: 10.1021/acs.biomac.6b00164
Biomacromolecules 2016, 17, 1536−1542

Table 3. Physical Properties of Mucus, as Calculated from FRAP Data[a]

particle size	time constant τ (10^{-3} s^{-1})	diffusion coefficient (10^{-13} m^2/s)	half time ($\tau_{1/2}$) s	calcd mobile particle fraction (A) %
100 nm	4.27 ± 1.0	4.2 ± 0.1	160 ± 40	24 ± 2
200 nm	1.16 ± 0.1	1.1 ± 0.02	600 ± 80	54 ± 5
500 nm	1.37 ± 0.5	1.3 ± 0.05	500 ± 200	14 ± 4

[a] n = 12, from four independent samples.

able to calculate and compare the diffusion coefficients to those obtained in the MPT experiments. Nevertheless, as indicated by the wide diffusion ranges obtained by MPT, the transport of nanoparticles through mucus appears to be much more complex than simple diffusion and may be better explained by short as well as long transient binding of the particles with the mucin matrix.[27,28] The unexpectedly low mobile fraction of the 100 nm particles may be explained by the assumption that these particles may get trapped within pores not accessible for the larger particles. This effect is well-known and even applied as a principle in gel exclusion chromatography (GPC), where large molecules pass through the separation columns faster than small ones. Still, a considerable fraction of the 200 nm particles can somehow access the previously bleached area. This implies that the heterogeneity of the pore size distribution within pulmonary mucus also allows somewhat larger particles eventually to find their way through pores that are compatible with their size.

2.4. Aerosol Deposition at the Air−Mucus Interface. Finally, in order to mimic the penetration of inhaled nanoparticles into the mucus gel layer, we deposited aerosolized nanoparticles onto mucus by means of a vibrating-mesh nebulizer. The aim of these experiments was to correlate the findings in terms of size dependent particle mobility observed during MPT and FRAP experiments, where the particles had been mechanically dispersed within the mucus gel, with a situation that is closer to the physiological scenario of inhaling such particles. Red-fluorescent, carboxylated polystyrene particles of 100, 200, and 500 nm could be successfully aerosolized, deposited, and detected on the surface of a thin layer of native pig pulmonary mucus. As expected, at t = 0 min, most of the particles were concentrated at the air−mucus interface, irrespective of their size (Figure 5A).

A total of 1 h later (t = 60 min), 500 nm particles were still unable to penetrate into the mucus layer at all and remained at the air−mucus interface (Figure 5). Remarkably, however, 200 nm particles also remained at the air−mucus interface, in contrast to the behavior of such particles when they are mechanically dispersed in mucus. This suggests that their penetration across the air-mucus interface is impeded, possibly by the lack of sufficiently large pores. Only 100 nm particles showed certain penetration into mucus, correlating well with the previously illustrated mobility within mucus.

Taking together, the results of this study suggest that there is a critical pore size that limits the penetration of nanoparticles into the mucus gel layer after aerosol deposition, which must be somewhere between 100 and 200 nm. These critically small pores ("micro-pores") are presumably located close to the air-mucus interface but connect to areas with much larger pores ("macro-pores") in the inner parts of the mucus layer. The mechanically dispersed particles were more equally distributed within the mucus layer, where the macro-pores are also located. This results in a much larger fraction of particles not restricted by micropores, which can freely diffuse on the length scales

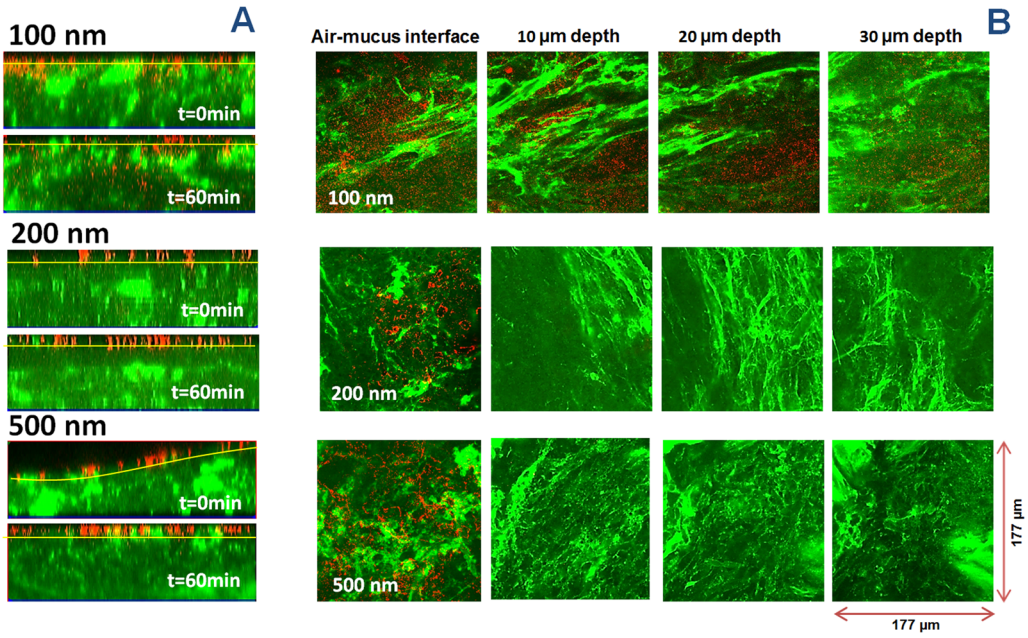

Figure 5. Confocal laser scanning microscopy study of the penetration of aerosolized 100, 200, and 500 nm red-fluorescent carboxylated nanoparticles through native porcine pulmonary mucus. Representative cross sections of 25−40 μm of the z-stacks captured at t = 0 min, directly after aerosol delivery of nanoparticles, and at t = 60 min, 1 h after aerosol delivery, are shown in A. Pulmonary mucus, in green, was stained with wheat germ agglutinin. Irrespective of their size, the particles were concentrated at the air−mucus interface (indicated by the yellow line) at t = 0 min. After 1 h, particle penetration through mucus was only apparent for 100 nm particles, whereas 200 and 500 nm particles remained at the air−mucus interface. Mucopenetration of 100 nm particles was accordingly observed in the micrographs at t = 60 min (177 μm × 177 μm) extracted from the z-stack at 10, 20, and 30 μm depths of the mucus layer (B); n = 3 measurements, each performed on an independent mucus sample.

DOI: 10.1021/acs.biomac.6b00164
Biomacromolecules 2016, 17, 1536−1542

observed by MPT and FRAP. Nonetheless, the limited penetration at the air-mucus interface could be due to a nanoparticle concentration-induced mucus fiber collapse, as reported by Lai et al.[1] In this study the authors reported that high concentrations of particles can make mucus fibers collapse into bundles. Once the mucin fibers collapse around particles, they can provide sufficient hydrophobic interactions to immobilize the particles. This scenario could apply after aerosol deposition of particles at the air-mucus interface.

CONCLUSION

Rheological measurements as well as FRAP and MPT experiments with polystyrene model particles of 100, 200, and 500 nm mechanically dispersed in vitro in native porcine pulmonary mucus suggest a heterogeneous mucus structure at a length scale between 100 and 1000 nm. The elastic regions of this gel exhibit different cross-linking densities with the mesh size potentially below 100 nm in some areas, but also contain larger interconnected pores with diameters in the range of 500 nm.

After aerosol deposition at the air−mucus interface, only particles of 100 nm, but not of 200 nm or larger, could penetrate into mucus. Such a penetration barrier can be best explained by a structure with micropores smaller than 200 nm and the absence of macro-pores close to the air-mucus interface. The even more strict size limit for particle penetration across the air-mucus interface compared to particle mobility within mucus provides another protective element of this important biological barrier to the exposure of inhaled nanoparticles that needs to be taken into account for the development of future inhalation nanomedicines.

ASSOCIATED CONTENT

Supporting Information

The Supporting Information is available free of charge on the ACS Publications website at DOI: 10.1021/acs.biomac.6b00164.

Calibration curves showing a strong linear correlation between the concentration and fluorescence intensity of the fluorescently labeled particles; Comparison of the MSD plots of 100, 200, and 500 nm carboxylated nanoparticles in fresh pulmonary pig mucus, versus pig mucus stored at −20 °C and thawed gradually (PDF).

Video-recording of 100 nm COOH-modified particles in native porcine pulmonary mucus (MPG).

Video-recording of 200 nm COOH-modified particles in native porcine pulmonary mucus (MPG).

Video-recording of 500 nm COOH-modified particles in native porcine pulmonary mucus (MPG).

AUTHOR INFORMATION

Corresponding Author

*E-mail: claus-michael.lehr@helmholtz-hzi.de. Tel.: +49 681 98806-1000.

Author Contributions

†These authors equally contributed to this work (X.M. and P.P.).

Notes

The authors declare no competing financial interest.

ACKNOWLEDGMENTS

This work was supported by the Marie Curie Initial Training Network PathChooser (PITNGA-2013−608373). The critical review of the manuscript performed by Dr. Sarah Gordon is gratefully acknowledged. The authors would like to thank Dr. Blatt and the team of the slaughterhouse in Zweibrücken for kindly providing airway samples.

REFERENCES

(1) Lai, S. K.; O'Hanlon, D. E.; Harrold, S.; Man, S. T.; Wang, Y. Y.; Cone, R.; Hanes, J. *Proc. Natl. Acad. Sci. U. S. A.* **2007**, *104*, 1482−1487.

(2) Nordgard, C. T.; Nonstad, U.; Olderoy, M. O.; Espevik, T.; Draget, K. I. *Biomacromolecules* **2014**, *15*, 2294−2300.

(3) Schuster, B. S.; Suk, J. S.; Woodworth, G. F.; Hanes, J. *Biomaterials* **2013**, *34*, 3439−3446.

(4) Knowles, M. R.; Boucher, R. C. *J. Clin. Invest.* **2002**, *109*, 571−577.

(5) Rubin, B. K. *Respir. Care* **2002**, *47*, 761−768.

(6) Lai, S. K.; Wang, Y. Y.; Hanes, J. *Adv. Drug Delivery Rev.* **2009**, *61*, 158−171.

(7) Ruge, C. A.; Kirch, J.; Lehr, C. M. *Lancet Respir. Med.* **2013**, *1*, 402−413.

(8) Hill, D. B.; Vasquez, P. A.; Mellnik, J.; McKinley, S. A.; Vose, A.; Mu, F.; Henderson, A. G.; Donaldson, S. H.; Alexis, N. E.; Boucher, R. C.; Forest, M. G. *PLoS One* **2014**, *9*, e87681.

(9) Khan, M. A.; Wolf, D. P.; Litt, M. *Biochim. Biophys. Acta, Gen. Subj.* **1976**, *444*, 369−373.

(10) Crater, J. S.; Carrier, R. L. *Macromol. Biosci.* **2010**, *10*, 1473−1483.

(11) Griessinger, J.; Dunnhaupt, S.; Cattoz, B.; Griffiths, P.; Oh, S.; Gomez, S. B.; Wilcox, M.; Pearson, J.; Gumbleton, M.; Bernkop-Schnurch, A. *Eur. J. Pharm. Biopharm.* **2015**, *96*, 464−476.

(12) Lai, S. K.; Wang, Y. Y.; Wirtz, D.; Hanes, J. *Adv. Drug Delivery Rev.* **2009**, *61*, 86−100.

(13) Lieleg, O.; Ribbeck, K. *Trends Cell Biol.* **2011**, *21*, 543−551.

(14) Sigurdsson, H. H.; Kirch, J.; Lehr, C. M. *Int. J. Pharm.* **2013**, *453*, 56−64.

(15) Macierzanka, A.; Mackie, A. R.; Bajka, B. H.; Rigby, N. M.; Nau, F.; Dupont, D. *PLoS One* **2014**, *9*, e95274.

(16) Dawson, M.; Wirtz, D.; Hanes, J. *J. Biol. Chem.* **2003**, *278*, 50393−50401.

(17) Yu, T.; Chan, K. W.; Anonuevo, A.; Song, X.; Schuster, B. S.; Chattopadhyay, S.; Xu, Q.; Oskolkov, N.; Patel, H.; Ensign, L. M.; van Zjil, P. C.; McMahon, M. T.; Hanes, J. *Nanomedicine* **2015**, *11*, 401−405.

(18) Kirch, J.; Schneider, A.; Abou, B.; Hopf, A.; Schaefer, U. F.; Schneider, M.; Schall, C.; Wagner, C.; Lehr, C. M. *Proc. Natl. Acad. Sci. U. S. A.* **2012**, *109*, 18355−18360.

(19) Forier, K.; Messiaen, A. S.; Raemdonck, K.; Deschout, H.; Rejman, J.; De Baets, F.; Nelis, H.; De Smedt, S. C.; Demeester, J.; Coenye, T.; Braeckmans, K. *Nanomedicine (London, U. K.)* **2013**, *8*, 935−949.

(20) Mura, S.; Hillaireau, H.; Nicolas, J.; Kerdine-Romer, S.; Le Droumaguet, B.; Delomenie, C.; Nicolas, V.; Pallardy, M.; Tsapis, N.; Fattal, E. *Biomacromolecules* **2011**, *12*, 4136−4143.

(21) Groo, A. C.; Lagarce, F. *Drug Discovery Today* **2014**, *19*, 1097−1108.

(22) Patton, J. S. *Adv. Drug Delivery Rev.* **1996**, *19*, 3−36.

(23) Kowalczyk, A.; Oelschlaeger, C.; Willenbacher, N. *Meas. Sci. Technol.* **2015**, *26*, 15302−15316.

(24) Innes, A. L.; Carrington, S. D.; Thornton, D. J.; Kirkham, S.; Rousseau, K.; Dougherty, R. H.; Raymond, W. W.; Caughey, G. H.; Muller, S. J.; Fahy, J. V. *Am. J. Respir. Crit. Care Med.* **2009**, *180*, 203−210.

(25) Sanders, N. N.; De Smedt, S. C.; Van Rompaey, E.; Simoens, P.; De Baets, F.; Demeester, J. *Am. J. Respir. Crit. Care Med.* **2000**, *162*, 1905−1911.

DOI: 10.1021/acs.biomac.6b00164
Biomacromolecules 2016, 17, 1536−1542

(26) Axelrod, D.; Koppel, D. E.; Schlessinger, J.; Elson, E.; Webb, W. W. *Biophys. J.* **1976**, *16*, 1055−1069.
(27) Phair, R. D.; Misteli, T. *Nat. Rev. Mol. Cell Biol.* **2001**, *2*, 898−907.
(28) Lippincott-Schwartz, J.; Altan-Bonnet, N.; Patterson, G. H. *Nat. Cell Biol.* **2003**, *Suppl*, S7−14.

DOI: 10.1021/acs.biomac.6b00164
Biomacromolecules 2016, 17, 1536−1542